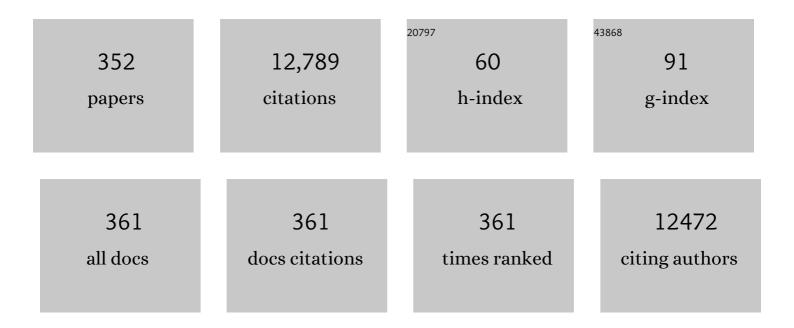
Guosheng Shao

List of Publications by Year in descending order

Source: https://exaly.com/author-pdf/7898412/publications.pdf Version: 2024-02-01



#	Article	IF	CITATIONS
1	An efficient room-temperature silicon-based light-emitting diode. Nature, 2001, 410, 192-194.	13.7	612
2	Two-dimensional Ruddlesden–Popper layered perovskite solar cells based on phase-pure thin films. Nature Energy, 2021, 6, 38-45.	19.8	342
3	Porous Carbons: Structureâ€Oriented Design and Versatile Applications. Advanced Functional Materials, 2020, 30, 1909265.	7.8	316
4	Phase Pure 2D Perovskite for Highâ€Performance 2D–3D Heterostructured Perovskite Solar Cells. Advanced Materials, 2018, 30, e1805323.	11.1	244
5	Buried Interfaces in Halide Perovskite Photovoltaics. Advanced Materials, 2021, 33, e2006435.	11.1	214
6	Mn-doped TiO2 nanopowders with remarkable visible light photocatalytic activity. Materials Letters, 2011, 65, 2051-2054.	1.3	195
7	Inkjet manipulated homogeneous large size perovskite grains for efficient and large-area perovskite solar cells. Nano Energy, 2018, 46, 203-211.	8.2	155
8	Red Shift in Manganese- and Iron-Doped TiO ₂ : A DFT+ <i>U</i> Analysis. Journal of Physical Chemistry C, 2009, 113, 6800-6808.	1.5	154
9	Oxidation of Nb–Si–Cr–Al in situ composites with Mo, Ti and Hf additions. Materials Science & Engineering A: Structural Materials: Properties, Microstructure and Processing, 2006, 441, 26-38.	2.6	146
10	A flexible metallic <scp>TiC</scp> nanofiber/vertical graphene <scp>1D</scp> / <scp>2D</scp> heterostructured as active electrocatalyst for advanced <scp>Li–S</scp> batteries. InformaÄnÃ- Materiály, 2021, 3, 790-803.	8.5	142
11	On the oxidation behaviour of MoSi2. Intermetallics, 2001, 9, 125-136.	1.8	137
12	Electronic Structures of Manganese-Doped Rutile TiO ₂ from First Principles. Journal of Physical Chemistry C, 2008, 112, 18677-18685.	1.5	135
13	Photogenerated Electron Transfer Process in Heterojunctions: In Situ Irradiation XPS. Small Methods, 2020, 4, 2000214.	4.6	129
14	Vertically aligned graphene nanosheets on multi-yolk/shell structured TiC@C nanofibers for stable Li–S batteries. Energy Storage Materials, 2020, 27, 159-168.	9.5	124
15	The formation of onion-like carbon-encapsulated cobalt carbide core/shell nanoparticles by the laser ablation of metallic cobalt in acetone. Carbon, 2013, 55, 108-115.	5.4	119
16	Recent Advances in Effective Reduction of Graphene Oxide for Highly Improved Performance Toward Electrochemical Energy Storage. Energy and Environmental Materials, 2018, 1, 5-12.	7.3	119
17	Pinecone biomass-derived hard carbon anodes for high-performance sodium-ion batteries. RSC Advances, 2017, 7, 41504-41511.	1.7	117
18	Construction of solid-state Z-scheme carbon-modified TiO2/WO3 nanofibers with enhanced photocatalytic hydrogen production. Journal of Power Sources, 2016, 328, 28-36.	4.0	114

#	Article	IF	CITATIONS
19	A study of the effects of Hf and Sn additions on the microstructure of Nbss/Nb5Si3 based in situ composites. Intermetallics, 2007, 15, 69-76.	1.8	110
20	Template-oriented synthesis of monodispersed SnS2@SnO2 hetero-nanoflowers for Cr(VI) photoreduction. Applied Catalysis B: Environmental, 2016, 192, 17-25.	10.8	108
21	Prediction of amorphous phase stability in the metal–silicon systems. Journal of Applied Physics, 2001, 90, 724-727.	1.1	107
22	Plasmon enhancement on photocatalytic hydrogen production over the Z-scheme photosynthetic heterojunction system. Applied Catalysis B: Environmental, 2017, 210, 297-305.	10.8	107
23	Prediction of phase selection in rapid solidification using time dependent nucleation theory. Acta Metallurgica Et Materialia, 1994, 42, 2937-2942.	1.9	104
24	Highly oriented Ge-doped hematite nanosheet arrays for photoelectrochemical water oxidation. Nano Energy, 2014, 9, 282-290.	8.2	104
25	Direct evidence of 2D/1D heterojunction enhancement on photocatalytic activity through assembling MoS2 nanosheets onto super-long TiO2 nanofibers. Applied Surface Science, 2020, 504, 144361.	3.1	100
26	One-dimensional Z-scheme TiO 2 /WO 3 /Pt heterostructures for enhanced hydrogen generation. Applied Surface Science, 2017, 391, 211-217.	3.1	99
27	Lithium–Sulfur Batteries Meet Electrospinning: Recent Advances and the Key Parameters for High Gravimetric and Volume Energy Density. Advanced Science, 2022, 9, e2103879.	5.6	98
28	Thermodynamic reassessment of the Mo–Si and Al–Mo–Si systems. Intermetallics, 2000, 8, 953-962.	1.8	96
29	Room temperature fabrication of p-channel Cu ₂ 0 thin-film transistors on flexible polyethylene terephthalate substrates. Applied Physics Letters, 2012, 101, 042114.	1.5	96
30	Electronic Properties of Rutile TiO ₂ with Nonmetal Dopants from First Principles. Journal of Physical Chemistry C, 2011, 115, 8274-8282.	1.5	92
31	Constructing 2D layered MoS 2 nanosheets-modified Z-scheme TiO 2 /WO 3 nanofibers ternary nanojunction with enhanced photocatalytic activity. Applied Surface Science, 2018, 430, 466-474.	3.1	92
32	The effects of Ti and Mo additions on the microstructure of Nb-silicide based in situ composites. Intermetallics, 2006, 14, 227-235.	1.8	91
33	Oneâ€Step Inkjet Printed Perovskite in Air for Efficient Light Harvesting. Solar Rrl, 2018, 2, 1700217.	3.1	90
34	Thermodynamic modelling of the Y–Zn and Mg–Zn–Y systems. Calphad: Computer Coupling of Phase Diagrams and Thermochemistry, 2006, 30, 286-295.	0.7	89
35	Microwave-assisted growth of In ₂ O ₃ nanoparticles on WO ₃ nanoplates to improve H ₂ S-sensing performance. Journal of Materials Chemistry A, 2014, 2, 18867-18874.	5.2	88
36	Normal-pressure microwave rapid synthesis of hierarchical SnO ₂ @rGO nanostructures with superhigh surface areas as high-quality gas-sensing and electrochemical active materials. Nanoscale, 2014, 6, 13690-13700.	2.8	88

#	Article	IF	CITATIONS
37	Low-temperature and highly selective NO-sensing performance of WO3 nanoplates decorated with silver nanoparticles. Sensors and Actuators B: Chemical, 2013, 185, 445-455.	4.0	86
38	Role of materials chemistry on the electrical/electronic properties of CuO thin films. Acta Materialia, 2015, 85, 122-131.	3.8	86
39	Ruddlesden–Popper Perovskite for Stable Solar Cells. Energy and Environmental Materials, 2018, 1, 221-231.	7.3	85
40	Enhanced performances of dye-sensitized solar cells based on Au-TiO 2 and Ag-TiO 2 plasmonic hybrid nanocomposites. Applied Surface Science, 2018, 430, 415-423.	3.1	84
41	Review—Research Progress on Layered Transition Metal Oxide Cathode Materials for Sodium Ion Batteries. Journal of the Electrochemical Society, 2021, 168, 050524.	1.3	82
42	Dye-sensitized solar cells based on TiO2 nanoparticles/nanobelts double-layered film with improved photovoltaic performance. Applied Surface Science, 2014, 319, 75-82.	3.1	78
43	Effect of Chromium and Niobium Doping on the Morphology and Electrochemical Performance of High-Voltage Spinel LiNi _{0.5} Mn _{1.5} O ₄ Cathode Material. ACS Applied Materials & Interfaces, 2016, 8, 9116-9124.	4.0	78
44	Dual Evolution in Defect and Morphology of Singleâ€Atom Dispersed Carbon Based Oxygen Electrocatalyst. Advanced Functional Materials, 2021, 31, 2010472.	7.8	78
45	From anti-perovskite to double anti-perovskite: tuning lattice chemistry to achieve super-fast Li ⁺ transport in cubic solid lithium halogen–chalcogenides. Journal of Materials Chemistry A, 2018, 6, 73-83.	5.2	77
46	Chemical bath deposited rutile TiO 2 compact layer toward efficient planar heterojunction perovskite solar cells. Applied Surface Science, 2017, 391, 337-344.	3.1	76
47	Work Function and Electron Affinity of Semiconductors: Doping Effect and Complication due to Fermi Level Pinning. Energy and Environmental Materials, 2021, 4, 273-276.	7.3	75
48	Enhancing efficiency of planar structure perovskite solar cells using Sn-doped TiO2 as electron transport layer at low temperature. Electrochimica Acta, 2018, 261, 227-235.	2.6	74
49	Effective promotion of spacial charge separation in direct Z-scheme WO3/CdS/WS2 tandem heterojunction with enhanced visible-light-driven photocatalytic H2 evolution. Chemical Engineering Journal, 2020, 398, 125602.	6.6	73
50	In situ sulfur-doped graphene nanofiber network as efficient metal-free electrocatalyst for polysulfides redox reactions in lithium–sulfur batteries. Journal of Energy Chemistry, 2020, 47, 281-290.	7.1	72
51	Theoretical design of solid electrolytes with superb ionic conductivity: alloying effect on Li ⁺ transportation in cubic Li ₆ PA ₅ X chalcogenides. Journal of Materials Chemistry A, 2017, 5, 21846-21857.	5.2	70
52	Ti ₃ C ₂ MXene as an "energy band bridge―to regulate the heterointerface mass transfer and electron reversible exchange process for Li–S batteries. Journal of Materials Chemistry A, 2020, 8, 25255-25267.	5.2	70
53	Rational Designs for Lithiumâ€Sulfur Batteries with Low Electrolyte/Sulfur Ratio. Advanced Functional Materials, 2021, 31, 2010499.	7.8	70
54	Synthesis and Ag-loading-density-dependent photocatalytic activity of Ag@TiO2 hybrid nanocrystals. Applied Surface Science, 2013, 284, 921-929.	3.1	69

#	Article	IF	CITATIONS
55	First Principle Material Genome Approach for All Solidâ€State Batteries. Energy and Environmental Materials, 2019, 2, 234-250.	7.3	69
56	Electronic properties of rutile TiO2 doped with 4d transition metals: First-principles study. Journal of Alloys and Compounds, 2013, 551, 118-124.	2.8	68
57	Mild solution-processed metal-doped TiO2 compact layers for hysteresis-less and performance-enhanced perovskite solar cells. Journal of Power Sources, 2017, 372, 235-244.	4.0	66
58	Thermodynamic assessment of the Nb–Si–Al system. Intermetallics, 2004, 12, 655-664.	1.8	65
59	Hierarchical Fe ₂ O ₃ @WO ₃ nanostructures with ultrahigh specific surface areas: microwave-assisted synthesis and enhanced H ₂ S-sensing performance. RSC Advances, 2015, 5, 328-337.	1.7	65
60	In Situ Fabrication of Nano Porous NiO-Capped Ni3P film as Anode for Li-Ion Battery with Different Lithiation Path and Significantly Enhanced Electrochemical Performance. Electrochimica Acta, 2016, 220, 258-266.	2.6	64
61	A novel reduction approach to fabricate quantum-sized SnO2-conjugated reduced graphene oxide nanocomposites as non-enzymatic glucose sensors. Physical Chemistry Chemical Physics, 2014, 16, 8801.	1.3	61
62	Effects of intensive forced melt convection on the mechanical properties of Fe containing Al–Si based alloys. Materials Science & Engineering A: Structural Materials: Properties, Microstructure and Processing, 2007, 445-446, 65-72.	2.6	60
63	Tracking charge transfer pathways in SrTiO3/CoP/Mo2C nanofibers for enhanced photocatalytic solar fuel production. Chinese Journal of Catalysis, 2022, 43, 507-518.	6.9	59
64	Molecular Beam Epitaxy Scalable Growth of Waferâ€Scale Continuous Semiconducting Monolayer MoTe ₂ on Inert Amorphous Dielectrics. Advanced Materials, 2019, 31, e1901578.	11.1	58
65	Prediction of amorphous phase stability in metallic alloys. Journal of Applied Physics, 2000, 88, 4443.	1.1	57
66	Origin of significant visible-light absorption properties of Mn-doped TiO2 thin films. Acta Materialia, 2012, 60, 1974-1985.	3.8	56
67	On the oxidation behavior of (Zr,Nb)2Fe under simulated nuclear reactor conditions. Corrosion Science, 2016, 112, 718-723.	3.0	55
68	Controllable construction of hierarchically CdIn2S4/CNFs/Co4S3 nanofiber networks towards photocatalytic hydrogen evolution. Chemical Engineering Journal, 2021, 419, 129213.	6.6	53
69	Polyethyleneimine High-Energy Hydrophilic Surface Interfacial Treatment toward Efficient and Stable Perovskite Solar Cells. ACS Applied Materials & Interfaces, 2016, 8, 32574-32580.	4.0	52
70	A "Threeâ€Region―Configuration for Enhanced Electrochemical Kinetics and Highâ€Areal Capacity Lithium–Sulfur Batteries. Advanced Functional Materials, 2022, 32, .	7.8	52
71	Thermodynamic modelling of the Cr–Nb–Si system. Intermetallics, 2005, 13, 69-78.	1.8	51
72	A thermo-gravimetric and microstructural study of the oxidation of Nbss/Nb5Si3-based in situ composites with Sn addition. Intermetallics, 2007, 15, 270-281.	1.8	51

#	Article	IF	CITATIONS
73	Amorphous-iron disilicide: A promising semiconductor. Applied Physics Letters, 2001, 79, 1438-1440.	1.5	50
74	Numerical study of metal oxide heterojunction solar cells. Semiconductor Science and Technology, 2011, 26, 085026.	1.0	49
75	Ge-doped hematite nanosheets with tunable doping level, structure and improved photoelectrochemical performance. Nano Energy, 2013, 2, 328-336.	8.2	49
76	Using iron fertilizer to control Cd accumulation in rice plants: A new promising technology. Science in China Series C: Life Sciences, 2008, 51, 245-253.	1.3	48
77	Spontaneous Growth and Chemical Reduction Ability of Ge Nanoparticles. Scientific Reports, 2013, 3, .	1.6	48
78	RGO-functionalized polymer nanofibrous membrane with exceptional surface activity and ultra-low airflow resistance for PM _{2.5} filtration. Environmental Science: Nano, 2018, 5, 1813-1820.	2.2	47
79	On the ω phase formation in Cr–Al and Ti–Al–Cr alloys. Acta Materialia, 2000, 48, 3671-3685.	3.8	46
80	Ultrafast solid-state lithium ion conductor through alloying induced lattice softening of Li ₆ PS ₅ Cl. Journal of Materials Chemistry A, 2018, 6, 19231-19240.	5.2	46
81	Multidimension ontrollable Synthesis of Ant Nestâ€5tructural Electrode Materials with Unique 3D Hierarchical Porous Features toward Electrochemical Applications. Advanced Functional Materials, 2019, 29, 1808994.	7.8	46
82	Reactive plasma deposition of high quality single phase CuO thin films suitable for metal oxide solar cells. Journal of Alloys and Compounds, 2017, 695, 3116-3123.	2.8	45
83	Construction of a low-defect and highly conductive 3D graphene network to enable a high sulphur content cathode for high performance Li–S/graphene batteries. Journal of Materials Chemistry A, 2018, 6, 22555-22565.	5.2	45
84	Reduced bilateral recombination by functional molecular interface engineering for efficient inverted perovskite solar cells. Nano Energy, 2020, 78, 105249.	8.2	45
85	Complex <scp>permittivityâ€dependent</scp> plasma <scp>confinementâ€assisted</scp> growth of asymmetric vertical graphene nanofiber membrane for <scp>highâ€performance Liâ€6</scp> full cells. InformaÄnÃ-MateriÄ¡ly, 2022, 4, .	8.5	45
86	Rheo-processing of an alloy specifically designed for semi-solid metal processing based on the Al–Mg–Si system. Materials Science & Engineering A: Structural Materials: Properties, Microstructure and Processing, 2008, 476, 341-349.	2.6	44
87	Limitation and extrapolation correction of the GGA + U formalism: a case study of Nb-doped anatase TiO2. Journal of Materials Chemistry C, 2013, 1, 3736.	2.7	44
88	Fabrication of Predominantly Mn ⁴⁺ â€Đoped TiO ₂ Nanoparticles under Equilibrium Conditions and Their Application as Visible‣ight Photocatalyts. Chemistry - an Asian Journal, 2014, 9, 1904-1912.	1.7	44
89	Nanoscale hybrid multidimensional perovskites with alternating cations for high performance photovoltaic. Nano Energy, 2019, 65, 104050.	8.2	44
90	Solvent-regulated solvothermal synthesis and morphology-dependent gas-sensing performance of low-dimensional tungsten oxide nanocrystals. Sensors and Actuators B: Chemical, 2014, 205, 391-400.	4.0	43

#	Article	IF	CITATIONS
91	Enabling remarkable cycling performance of high-loading MoS2@Graphene anode for sodium ion batteries with tunable cut-off voltage. Journal of Power Sources, 2020, 458, 228040.	4.0	43
92	Enabling Argyrodite Sulfides as Superb Solid‣tate Electrolyte with Remarkable Interfacial Stability Against Electrodes. Energy and Environmental Materials, 2022, 5, 852-864.	7.3	43
93	ω-phase formation in V[sbnd]Al and Ti[sbnd]Al[sbnd]V alloys. Philosophical Magazine A: Physics of Condensed Matter, Structure, Defects and Mechanical Properties, 1995, 71, 1389-1408.	0.7	42
94	Study of three-phase equilibrium in the Nb-rich corner of Nb–Si–Cr system. Intermetallics, 2006, 14, 832-837.	1.8	42
95	Mn-doped TiO ₂ thin films with significantly improved optical and electrical properties. Journal Physics D: Applied Physics, 2012, 45, 485102.	1.3	42
96	Remote plasma sputtering deposited Nb-doped TiO2 with remarkable transparent conductivity. Solar Energy Materials and Solar Cells, 2016, 149, 310-319.	3.0	40
97	Synthesis of transition metal oxide nanoparticles with ultrahigh oxygen adsorption capacity and efficient catalytic oxidation performance. Journal of Materials Chemistry, 2009, 19, 6097.	6.7	39
98	Fabrication and photovoltaic performance of niobium doped TiO2 hierarchical microspheres with exposed {001} facets and high specific surface area. Applied Surface Science, 2017, 410, 241-248.	3.1	39
99	A theoretical approach to address interfacial problems in all-solid-state lithium ion batteries: tuning materials chemistry for electrolyte and buffer coatings based on Li ₆ PA ₅ Cl hali-chalcogenides. Journal of Materials Chemistry A, 2019, 7, 5239-5247.	5.2	39
100	Large-scale synthesis and enhanced visible-light-driven photocatalytic performance of hierarchical Ag/AgCl nanocrystals derived from freeze-dried PVP–Ag+ hybrid precursors with porosity. Applied Catalysis B: Environmental, 2014, 144, 394-407.	10.8	38
101	Lithium Ion Conductivity in Double Antiperovskite Li _{6.5} OS _{1.5} I _{1.5} : Alloying and Boundary Effects. ACS Applied Energy Materials, 2019, 2, 6288-6294.	2.5	38
102	A mechanism assessment for the anti-corrosion of zirconia coating under the condition of subcritical water corrosion. Corrosion Science, 2019, 152, 54-59.	3.0	38
103	Multilevel polarization-fields enhanced capture and photocatalytic conversion of particulate matter over flexible schottky-junction nanofiber membranes. Journal of Hazardous Materials, 2020, 395, 122639.	6.5	38
104	Stable all-solid-state battery enabled with Li6.25PS5.25Cl0.75 as fast ion-conducting electrolyte. Journal of Energy Chemistry, 2021, 53, 147-154.	7.1	38
105	Regulation of energetic hot carriers on Pt/TiO2 with thermal energy for photothermal catalysis. Applied Catalysis B: Environmental, 2022, 309, 121263.	10.8	38
106	Durable self-polishing antifouling Cu-Ti coating by a micron-scale Cu/Ti laminated microstructure design. Journal of Materials Science and Technology, 2021, 79, 62-74.	5.6	37
107	Pinning Bromide Ion with Ionic Liquid in Leadâ€Free Cs ₂ AgBiBr ₆ Double Perovskite Solar Cells. Advanced Functional Materials, 2022, 32, .	7.8	37
108	Theoretical design of double anti-perovskite Na ₆ SOI ₂ as a super-fast ion conductor for solid Na ⁺ ion batteries. Journal of Materials Chemistry A, 2018, 6, 19843-19852.	5.2	36

#	Article	IF	CITATIONS
109	Thermodynamic and kinetic aspects of intermetallic amorphous alloys. Intermetallics, 2003, 11, 313-324.	1.8	35
110	Structural engineering of thin films of vertically aligned TiO2 nanorods. Materials Letters, 2010, 64, 1614-1617.	1.3	35
111	Three-dimensional Porous Networks of Ultra-long Electrospun SnO2 Nanotubes with High Photocatalytic Performance. Nano-Micro Letters, 2015, 7, 86-95.	14.4	35
112	X-ray photoelectron spectroscopy studies of Ti-Al and Ti-Al-V alloys using Cr K? radiation. Surface and Interface Analysis, 2001, 31, 734-744.	0.8	34
113	Phase selection and visible light photo-catalytic activity of Fe-doped TiO2 prepared by the hydrothermal method. Materials Research Bulletin, 2011, 46, 442-446.	2.7	34
114	P2-type Na _{2/3} Ni _{1/3} Mn _{2/3} O ₂ Cathode Material with Excellent Rate and Cycling Performance for Sodium-Ion Batteries. Journal of the Electrochemical Society, 2019, 166, A3980-A3986.	1.3	34
115	Functional carbon nitride materials for water oxidation: from heteroatom doping to interface engineering. Nanoscale, 2020, 12, 6937-6952.	2.8	34
116	Solidification structures of Ti–Al–Cr alloys. Intermetallics, 1999, 7, 579-587.	1.8	33
117	Electronic structure and bonding inMo3Si,Mo5Si3, andMo(Si,Al)2alloys investigated by x-ray photoelectron spectroscopy and density-functional theory. Physical Review B, 2005, 71, .	1.1	33
118	Investigation of the hydrogen bonding in ice Ih by first-principles density function methods. Journal of Chemical Physics, 2012, 137, 044504.	1.2	33
119	Covalently Connecting Crystal Grains with Polyvinylammonium Carbochain Backbone To Suppress Grain Boundaries for Long-Term Stable Perovskite Solar Cells. ACS Applied Materials & Interfaces, 2017, 9, 6064-6071.	4.0	33
120	High-capacity cathodes for magnesium lithium chlorine tri-ion batteries through chloride intercalation in layered MoS ₂ : a computational study. Journal of Materials Chemistry A, 2018, 6, 6830-6839.	5.2	33
121	First principles study for band engineering of KNbO ₃ with 3d transition metal substitution. RSC Advances, 2019, 9, 7551-7559.	1.7	33
122	Simultaneously boost diffusion length and stability of perovskite for high performance solar cells. Nano Energy, 2019, 59, 721-729.	8.2	33
123	Calculations of charge transfer in Nb–17Al and V–50Al alloys, using the Auger parameter. Intermetallics, 1999, 7, 937-946.	1.8	32
124	The formation and stacking faults of Fe and Cr containing Laves phase in Zircaloy-4 alloy. Materials Letters, 2017, 191, 203-205.	1.3	32
125	Enhanced efficiency and stability of perovskite solar cells by 2D perovskite vapor-assisted interface optimization. Journal of Energy Chemistry, 2020, 45, 103-109.	7.1	32
126	Nano-porous hollow Li _{0.5} La _{0.5} TiO ₃ spheres and electronic structure modulation for ultra-fast H ₂ S detection. Journal of Materials Chemistry A, 2020, 8, 2376-2386.	5.2	32

#	Article	IF	CITATIONS
127	Computational design of high efficiency FeSi2 thin-film solar cells. Thin Solid Films, 2011, 519, 8490-8495.	0.8	31
128	The effect of cobalt doping on the morphology and electrochemical performance of high-voltage spinel LiNi0.5Mn1.5O4 cathode material. Solid State Ionics, 2016, 292, 70-74.	1.3	31
129	Simulation of planar Si/Mg 2 Si/Si p-i-n heterojunction solar cells for high efficiency. Solar Energy, 2017, 158, 654-662.	2.9	31
130	Synergistic Cooperation of Rutile TiO ₂ {002}, {101}, and {110} Facets for Hydrogen Sensing. ACS Applied Materials & Interfaces, 2018, 10, 28199-28209.	4.0	31
131	Synergistic effect of cation ordered structure and grain boundary engineering on long-term cycling of Li0.35La0.55TiO3-based solid batteries. Journal of the European Ceramic Society, 2019, 39, 3332-3337.	2.8	31
132	In-plane grain boundary induced defect state in hierarchical NiCo-LDH and effect on battery-type charge storage. Nano Research, 2023, 16, 4908-4916.	5.8	31
133	Is there a future for semiconducting silicides? (invited). Microelectronic Engineering, 2000, 50, 223-235.	1.1	30
134	Effect of implantation temperature on dislocation loop formation and origin of 1.55-î¼m photoluminescence from ion-beam-synthesized FeSi2 precipitates in silicon. Applied Physics Letters, 2003, 83, 42-44.	1.5	30
135	The effects of electron and hole transport layer with the electrode work function on perovskite solar cells. Modern Physics Letters B, 2016, 30, 1650341.	1.0	30
136	Fundamental Basis for Distinctive Sensing of H ₂ in Humid Environment. Energy and Environmental Materials, 2018, 1, 174-178.	7.3	30
137	Nitrogen-doped vertical graphene nanosheets by high-flux plasma enhanced chemical vapor deposition as efficient oxygen reduction catalysts for Zn–air batteries. Journal of Materials Chemistry A, 2020, 8, 23248-23256.	5.2	30
138	In Situ Electrochemical Intercalationâ€Induced Phase Transition to Enhance Catalytic Performance for Lithium–Sulfur Battery. Small, 2021, 17, e2100065.	5.2	30
139	Efficient silicon light emitting diodes made by dislocation engineering. Physica E: Low-Dimensional Systems and Nanostructures, 2003, 16, 376-381.	1.3	29
140	Accelerating directional charge separation via built-in interfacial electric fields originating from work-function differences. Chinese Journal of Catalysis, 2021, 42, 583-594.	6.9	29
141	Metastability of the o-phase in transition-metal aluminides: First-principles structural predictions. Philosophical Magazine A: Physics of Condensed Matter, Structure, Defects and Mechanical Properties, 1996, 74, 1385-1397.	0.7	28
142	On the crystallographic characteristics of ion beam synthesised β–FeSi2. Intermetallics, 2000, 8, 1405-1412.	1.8	28
143	Thermodynamic assessment of the Ru–Si and Os–Si systems. Journal of Alloys and Compounds, 2001, 320, 72-79.	2.8	28
144	Ion beam synthesis of superconducting MgB2 thin films. Applied Physics Letters, 2003, 82, 236-238.	1.5	28

#	Article	IF	CITATIONS
145	On the solidification microstructure of Mg–30Zn–2.5Y metal–intermetallic alloy. Intermetallics, 2006, 14, 596-602.	1.8	28
146	Strong interplay between dopant and SnO2 in amorphous transparent (Sn, Nb)O2 anode with high conductivity in electrochemical cycling. Journal of Alloys and Compounds, 2018, 735, 2401-2409.	2.8	28
147	Surficial Structure Retention Mechanism for LiNi _{0.8} Co _{0.15} Al _{0.05} O ₂ in a Full Gradient Cathode. ACS Applied Materials & Interfaces, 2019, 11, 31991-31996.	4.0	28
148	Engineering of boron-induced dislocation loops for efficient room-temperature silicon light-emitting diodes. Journal of Applied Physics, 2005, 97, 073512.	1.1	27
149	Glass forming ability of multi-component metallic systems. Intermetallics, 2005, 13, 409-414.	1.8	27
150	Remarkable optical red shift and extremely high optical absorption coefficient of V-Ga co-doped TiO2. Journal of Applied Physics, 2012, 112, .	1.1	27
151	Theoretical tuning of Ruddlesden–Popper type anti-perovskite phases as superb ion conductors and cathodes for solid sodium ion batteries. Journal of Materials Chemistry A, 2019, 7, 10483-10493.	5.2	27
152	3D CuO Network Supported TiO ₂ Nanosheets with Applications for Energy Storage and Water Splitting. Science of Advanced Materials, 2016, 8, 1256-1262.	0.1	27
153	Synthesis of amorphous FeSi2 by ion beam mixing. Nuclear Instruments & Methods in Physics Research B, 2002, 188, 166-169.	0.6	26
154	On the role of dislocation loops in silicon light emitting diodes. Applied Physics Letters, 2005, 87, 201105.	1.5	26
155	Self-aligned TiO2 thin films with remarkable hydrogen sensing functionality. Sensors and Actuators B: Chemical, 2012, 171-172, 165-171.	4.0	26
156	Enhanced thermoelectric performance via randomly arranged nanopores: Excellent transport properties of YbZn2Sb2 nanoporous materials. Acta Materialia, 2012, 60, 1741-1746.	3.8	26
157	In Situ Monitored (N, O)â€Doping of Flexible Vertical Graphene Films with Highâ€Flux Plasma Enhanced Chemical Vapor Deposition for Remarkable Metalâ€Free Redox Catalysis Essential to Alkaline Zinc–Air Batteries. Advanced Science, 2022, 9, e2200614.	5.6	26
158	Transition from amorphous to crystalline beta phase in co-sputtered FeSi2 films as a function of temperature. Journal of Applied Physics, 2005, 98, 123506.	1.1	25
159	Interplay between Ag and interstitial Mg on the p-type characteristics of Ag-doped Mg2Si: challenges for high hole conductivity. Journal of Materials Chemistry C, 2015, 3, 530-537.	2.7	25
160	Facile assembly of partly graphene-enveloped sulfur composites in double-solvent for lithium–sulfur batteries. Electrochimica Acta, 2015, 178, 564-570.	2.6	25
161	Theoretical formulation of Na ₃ AO ₄ X (A = S/Se, X = F/Cl) as high-performance solid electrolytes for all-solid-state sodium batteries. Journal of Materials Chemistry A, 2019, 7, 21985-21996.	5.2	25
162	Integrated structural design of polyaniline-modified nitrogen-doped hierarchical porous carbon nanofibers as binder-free electrodes toward all-solid-state flexible supercapacitors. Applied Surface Science, 2020, 501, 144001.	3.1	25

#	Article	IF	CITATIONS
163	Enhancement of Interfacial Charge Transportation Through Construction of 2D–2D p–n Heterojunctions in Hierarchical 3D CNFs/MoS ₂ /ZnIn ₂ S ₄ Composites to Enable Highâ€Efficiency Photocatalytic Hydrogen Evolution. Solar Rrl, 2021, 5, 2000722.	3.1	25
164	Metastable \hat{I}^3 phase in ion beam synthesized FeSi2. Applied Physics Letters, 1996, 68, 1784-1786.	1.5	24
165	Numerical study of metal oxide Schottky type solar cells. Solid State Sciences, 2012, 14, 857-863.	1.5	24
166	Lightâ€Induced Ion Rectification in Zigzag Nanochannels. Chemistry - an Asian Journal, 2015, 10, 2733-2737.	1.7	24
167	A designer fast Li-ion conductor Li6.25PS5.25Cl0.75 and its contribution to the polyethylene oxide based electrolyte. Applied Surface Science, 2019, 493, 1326-1333.	3.1	24
168	High-efficiency perovskite solar cells based on self-assembly n-doped fullerene derivative with excellent thermal stability. Journal of Power Sources, 2019, 413, 459-466.	4.0	24
169	"Room-like―TiO ₂ Array as a Sulfur Host for Lithium-Sulfur Batteries: Combining Advantages of Array and Closed Structures. ACS Sustainable Chemistry and Engineering, 2020, 8, 7609-7616.	3.2	24
170	A simple synthesis of magnetic metal implanted hierarchical porous carbon networks for efficient microwave absorption. Journal of Materials Chemistry C, 2021, 9, 14866-14875.	2.7	24
171	Prediction of structural stabilities of transition-metal disilicide alloys by the density functional theory. Acta Materialia, 2005, 53, 3729-3736.	3.8	23
172	Formation of nanocrystalline δ-ZrH x in Zircoloy-4: Orientation relationship and twinning. Journal of Alloys and Compounds, 2016, 658, 494-499.	2.8	23
173	Controlling the film structure by regulating 2D Ruddlesden–Popper perovskite formation enthalpy for efficient and stable tri-cation perovskite solar cells. Journal of Materials Chemistry A, 2020, 8, 5874-5881.	5.2	23
174	Rational regulation on charge spatial separation and directional migration in the yolk-shell structural SiO2/Ni2P/rGO/Cd0.5Zn0.5S nanoreactor for efficient photocatalytic H2 evolution. Chemical Engineering Journal, 2021, 404, 126497.	6.6	23
175	Atomic Layer Coated Al ₂ O ₃ on Nitrogen Doped Vertical Graphene Nanosheets for High Performance Sodium Ion Batteries. Energy and Environmental Materials, 2022, 5, 285-294.	7.3	23
176	Near solution-level conductivity of polyvinyl alcohol based electrolyte and the application for fully compliant Al-air battery. Chemical Engineering Journal, 2022, 431, 134283.	6.6	23
177	In situ formation of Au/SnO 2 nanocrystals on WO 3 nanoplates as excellent gas-sensing materials for H 2 S detection. Materials Chemistry and Physics, 2014, 148, 1099-1107.	2.0	22
178	Direct evidence of multichannel-improved charge-carrier mechanism for enhanced photocatalytic H2 evolution. Scientific Reports, 2017, 7, 16116.	1.6	22
179	High-quality rGO/MoS2 composite via a facile "prereduction-microwave―strategy for enhanced lithium and sodium storage. Journal of Alloys and Compounds, 2020, 821, 153207.	2.8	22
180	Self-consistent assessment of Li+ ion cathodes: Theory vs. experiments. Journal of Energy Chemistry, 2021, 59, 229-241.	7.1	22

#	Article	IF	CITATIONS
181	Role of nucleation in phase competition in binary Ti-Al alloys. Materials Science and Technology, 1997, 13, 797-805.	0.8	21
182	Thermodynamic assessment of the Hf–Mo and Hf–W systems. Intermetallics, 2002, 10, 429-434.	1.8	21
183	Prediction of ω phase formation in Ti–Al–X alloys. Materials Science & Engineering A: Structural Materials: Properties, Microstructure and Processing, 2002, 329-331, 914-919.	2.6	21
184	Silicon-based light emitting devices. Vacuum, 2005, 78, 551-556.	1.6	21
185	Molecular-dynamics simulations of binary Pd-Si metal alloys: Glass formation, crystallisation and cluster properties. Journal of Non-Crystalline Solids, 2018, 487, 72-86.	1.5	21
186	Chemical diversity of iron species and structure evolution during the oxidation of C14 Laves phase Zr(Fe,Nb)2 in subcritical environment. Corrosion Science, 2020, 162, 108218.	3.0	21
187	Semiconducting amorphous FeSi2 layers synthesized by co-sputter deposition. Thin Solid Films, 2004, 461, 72-76.	0.8	20
188	Molecular Design of TiO ₂ for Gigantic Red Shift via Sublattice Substitution. Journal of Nanoscience and Nanotechnology, 2010, 10, 7092-7096.	0.9	20
189	Enhanced selective response to nitric oxide (NO) of Au-modified tungsten trioxide nanoplates. Materials Chemistry and Physics, 2013, 143, 461-469.	2.0	20
190	Simultaneous doping and growth of Sn-doped hematite nanocrystalline films with improved photoelectrochemical performance. RSC Advances, 2014, 4, 63408-63413.	1.7	20
191	Significant Influences of Elaborately Modulating Electron Donors on Light Absorption and Multichannel Charge-Transfer Dynamics for 4-(Benzo[<i>c</i>][1,2,5]thiadiazol-4-ylethynyl)benzoic Acid Dyes. ACS Applied Materials & Interfaces, 2016, 8, 18292-18300.	4.0	20
192	Mechanistic investigations of N-doped graphene/2H(1T)-MoS2 for Li/K-ions batteries. Nano Energy, 2020, 78, 105352.	8.2	20
193	Theoretical identification of layered MXene phase Na _x Ti ₄ C ₂ O ₄ as superb anodes for rechargeable sodium-ion batteries. Journal of Materials Chemistry A, 2020, 8, 11177-11187.	5.2	20
194	Confining sulfur in intact freestanding scaffold of yolk-shell nanofibers with high sulfur content for lithium-sulfur batteries. Journal of Energy Chemistry, 2020, 51, 378-387.	7.1	20
195	On optical reflection at heterojunction interface of thin film solar cells. Solar Energy Materials and Solar Cells, 2013, 111, 141-145.	3.0	19
196	Numerical study of metal oxide hetero-junction solar cells with defects and interface states. Semiconductor Science and Technology, 2013, 28, 055004.	1.0	19
197	Complex doping chemistry owing to Mn incorporation in nanocrystalline anatase TiO ₂ powders. Physical Chemistry Chemical Physics, 2016, 18, 2818-2829.	1.3	19
198	Order domain boundaries in ion beam synthesized semiconducting FeSi2 layers. Applied Physics Letters, 1995, 67, 667-669.	1.5	18

#	Article	IF	CITATIONS
199	Strong temperature-dependent crystallization, phase transition, optical and electrical characteristics of p-type CuAlO ₂ thin films. Physical Chemistry Chemical Physics, 2015, 17, 557-562.	1.3	18
200	Fundamental Pathways for the Adsorption and Transport of Hydrogen on TiO ₂ Surfaces: Origin for Effective Sensing at about Room Temperature. ACS Applied Materials & Interfaces, 2016, 8, 35298-35307.	4.0	18
201	Formation and fine-structures of nano-precipitates in ZIRLO. Journal of Alloys and Compounds, 2016, 687, 451-457.	2.8	18
202	Suppression on allotropic transformation of Sn planar anode with enhanced electrochemical performance. Applied Surface Science, 2018, 435, 1150-1158.	3.1	18
203	Sputtered Ga-Doped SnO _{<i>x</i>} Electron Transport Layer for Large-Area All-Inorganic Perovskite Solar Cells. ACS Applied Materials & Interfaces, 2020, 12, 54904-54915.	4.0	18
204	Recent Progress in Perovskiteâ€Based Reversible Photon–Electricity Conversion Devices. Advanced Functional Materials, 2022, 32, 2108926.	7.8	18
205	Ordering and decomposition of the β phase in melt-spun TiAl1 â^' x Vx alloys. Materials Science & Engineering A: Structural Materials: Properties, Microstructure and Processing, 1996, 216, 1-10.	2.6	17
206	Calculations of charge transfer in Mg-and Al-transition metal alloys using the Auger parameter. Surface and Interface Analysis, 2000, 29, 65-72.	0.8	17
207	Phase selection in magnetron sputter-deposited TiAl alloy. Materials Science & Engineering A: Structural Materials: Properties, Microstructure and Processing, 2002, 329-331, 141-146.	2.6	17
208	Crystallization of the amorphous Fe80Zr12B8 alloy under controlled heating. Journal of Alloys and Compounds, 2008, 459, 185-190.	2.8	17
209	Phase transformations in Ti-40Al-10V. Intermetallics, 1995, 3, 315-325.	1.8	16
210	Beta phase decomposition in Nb—17 at.% Al alloy. Philosophical Magazine A: Physics of Condensed Matter, Structure, Defects and Mechanical Properties, 1997, 75, 637-655.	0.7	16
211	Lattice parameters of TM(3d)–Al solid solutions. Materials Science & Engineering A: Structural Materials: Properties, Microstructure and Processing, 1999, 271, 286-290.	2.6	16
212	Improving high-temperature oxidation resistance of TiAl-based alloys by MnCl2 surface treatment. Intermetallics, 2003, 11, 651-660.	1.8	16
213	Ion beam synthesized silicides: growth, characterization and devices. Thin Solid Films, 2001, 381, 188-193.	0.8	15
214	Transmission electron microscopy observation of high-temperature Î ³ -FeSi2 precipitates formed in Si by iron implantation using a metal vapor vacuum arc ion source. Applied Physics Letters, 2003, 83, 638-640.	1.5	15
215	Origin of <i>n</i> -type conductivity of Sn-doped Mg2Si from first principles. Journal of Applied Physics, 2012, 112, .	1.1	15
216	SnO2-core carbon-shell composite nanotubes with enhanced photocurrent and photocatalytic performance. Applied Catalysis B: Environmental, 2015, 166-167, 193-201.	10.8	15

#	Article	IF	CITATIONS
217	Bio-inspired construction of electrocatalyst decorated hierarchical porous carbon nanoreactors with enhanced mass transfer ability towards rapid polysulfide redox reactions. Nano Research, 2021, 14, 3942-3951.	5.8	15
218	Array-Structured Double-Ion Cooperative Adsorption Sites as Multifunctional Sulfur Hosts for Lithium–Sulfur Batteries with Low Electrolyte/Sulfur Ratio. ACS Nano, 2021, 15, 16322-16334.	7.3	15
219	In situ atomic-scale engineering of the chemistry and structure of the grain boundaries region of Li3La2/3-TiO3. Scripta Materialia, 2020, 185, 134-139.	2.6	15
220	Formulation of Li-metal-halide (LMX) solid state electrolytes through extensive first principles modelling. Journal of Materials Chemistry A, 2021, 9, 25585-25594.	5.2	15
221	On the structural evolution of Fe-Al laminates obtained by physical vapour deposition. Philosophical Magazine A: Physics of Condensed Matter, Structure, Defects and Mechanical Properties, 2000, 80, 693-710.	0.7	14
222	PbS QDs as Electron Blocking Layer Toward Efficient and Stable Perovskite Solar Cells. IEEE Journal of Photovoltaics, 2019, 9, 194-199.	1.5	14
223	Two-pronged approach to regulate Li etching for a stable anode. Journal of Power Sources, 2020, 455, 227988.	4.0	14
224	Synthesis of a Visibleâ€Lightâ€Responsive Perovskite SmTiO ₂ N Bifunctional Photocatalyst via an Evaporationâ€Assisted Layeredâ€Precursor Strategy. Advanced Materials, 2021, 33, e2101883.	11.1	14
225	Significant performance enhancement of allâ€inorganic CsPbBr ₃ perovskite solar cells enabled by Nbâ€doped SnO ₂ as effective electron transport layer. Energy and Environmental Materials, 2021, 4, 671-680.	7.3	14
226	The metastable disordered γ (TiAl) phase and its ordering process in a rapidly solidified equiatomic TiAl alloy with vanadium addition. Scripta Metallurgica Et Materialia, 1994, 30, 809-814.	1.0	13
227	A study of alloying behaviour in the Ti–Al–V system. Acta Materialia, 2002, 50, 1951-1960.	3.8	13
228	Optimising dislocation-engineered silicon light-emitting diodes. Applied Physics B: Lasers and Optics, 2006, 83, 289-294.	1.1	13
229	Boron engineered dislocation loops for efficient room temperature silicon light emitting diodes. Thin Solid Films, 2006, 504, 36-40.	0.8	13
230	Vertically aligned smooth ZnO nanorod films for planar device applications. Journal of Materials Chemistry C, 2013, 1, 2525.	2.7	13
231	<i>In situ</i> coupling of Ti ₂ 0 with rutile TiO ₂ as a core–shell structure and its photocatalysis performance. RSC Advances, 2017, 7, 54662-54667.	1.7	13
232	Direct Growth of Vertically Aligned Carbon Nanotubes onto Transparent Conductive Oxide Glass for Enhanced Charge Extraction in Perovskite Solar Cells. Advanced Materials Interfaces, 2020, 7, 2001121.	1.9	13
233	Mechanism of enhanced H2S sensor ability based on emerging Li0.5La0.5TiO3-SnO2 core-shell structure. Sensors and Actuators B: Chemical, 2022, 352, 131054.	4.0	13
234	Watermelon Peelâ€Derived Nitrogenâ€Doped Porous Carbon as a Superior Oxygen Reduction Electrocatalyst for Zincâ€Air Batteries. ChemElectroChem, 2021, 8, 4790-4796.	1.7	13

#	Article	IF	CITATIONS
235	Ion beam synthesized Ru2Si3. Applied Physics Letters, 1999, 75, 1282-1283.	1.5	12
236	TEM study of self-assembled FeSi2 nanostructures by ion beam implantation. Solid State Communications, 2009, 149, 97-100.	0.9	12
237	Novel ZnO nanorod films by chemical solution deposition for planar device applications. Nanotechnology, 2013, 24, 275601.	1.3	12
238	Stable high-performance perovskite solar cells based on inorganic electron transporting bi-layers. Nanotechnology, 2018, 29, 385401.	1.3	12
239	Theoretical formulation of Li _{3a+b} N _a X _b (X = halogen) as a potential artificial solid electrolyte interphase (ASEI) to protect the Li anode. Physical Chemistry Chemical Physics, 2020, 22, 12918-12928.	1.3	12
240	Dynamic Reaction Mechanism of P–N-Switched H ₂ -Sensing Performance on a Pt-Decorated TiO ₂ Surface. ACS Applied Materials & Interfaces, 2021, 13, 25472-25482.	4.0	12
241	Effect of Ge concentration on the propagation characteristics of SiGe/Si heterojunction waveguides. Journal of Applied Physics, 1995, 77, 2254-2257.	1.1	11
242	Dislocation engineered Î ² -FeSi2 light emitting diodes. Nuclear Instruments & Methods in Physics Research B, 2003, 206, 436-439.	0.6	11
243	Ion beam fabricated silicon light emitting diodes. Physica Status Solidi A, 2004, 201, 239-244.	1.7	11
244	Theoretical prediction of p-type transparent conductivity in Zn-doped TiO2. Physical Chemistry Chemical Physics, 2013, 15, 9581.	1.3	11
245	Reactive vapor deposition and electrochemical performance of nano-structured magnesium silicide on silicon and silicon carbide substrates. Materials Science in Semiconductor Processing, 2014, 27, 873-876.	1.9	11
246	Freeze-dried PVP–Ag+ precursors to novel AgBr/AgCl–Ag hybrid nanocrystals for visible-light-driven photodegradation of organic pollutants. Superlattices and Microstructures, 2015, 80, 136-150.	1.4	11
247	Improved hydrogen sensing of (004) oriented anatase TiO2 thin films through post annealing. International Journal of Hydrogen Energy, 2019, 44, 20606-20615.	3.8	11
248	Size effect on the electrochemical reaction path and performance of nano size phosphorus rich skutterudite nickle phosphide. Journal of Alloys and Compounds, 2019, 781, 1059-1068.	2.8	11
249	Entropy Change Characteristics of the LiNi _{0.5} Mn _{1.5} O ₄ Cathode Material for Lithium-Ion Batteries. ACS Omega, 2020, 5, 4109-4114.	1.6	11
250	In-situ hydrogen production and storage in (0Â0Â2) oriented TiO2 thin films. Applied Surface Science, 2020, 509, 145366.	3.1	11
251	Transport of Sodium Ions in Solids: Progress in Firstâ€Principle Theoretical Formulation of Potential Solid Sodiumâ€Ion Electrolytes. Batteries and Supercaps, 2021, 4, 1096-1107.	2.4	11
252	Phase transformations in Nb-17Al-xMo alloys. Intermetallics, 1997, 5, 203-219.	1.8	10

#	Article	IF	CITATIONS
253	Thermodynamic analysis of the Re–Si system. Intermetallics, 2001, 9, 1063-1068.	1.8	10
254	Characterization and light emission properties of β-FeSi2 precipitates in Si synthesized by metal vapor vacuum arc ion implantation. Nuclear Instruments & Methods in Physics Research B, 2003, 206, 317-320.	0.6	10
255	Microstructural and Optical Properties of Semiconducting MnSi1.7Synthesized by Ion Implantation. Japanese Journal of Applied Physics, 2007, 46, 5777-5779.	0.8	10
256	Correlation of Structural and Optical Properties of Sputtered FeSi2Thin Films. Japanese Journal of Applied Physics, 2010, 49, 081401.	0.8	10
257	Dominant growth of higher manganese silicide film on Si substrate by introducing a Si oxide capping layer. Journal of Alloys and Compounds, 2018, 740, 541-544.	2.8	10
258	"Mechanical–electrochemical―coupling structure and the application as a three-dimensional current collector for lithium metal anode. Applied Surface Science, 2021, 563, 150247.	3.1	10
259	Ϊ‰-phase formation in a rapidly solidified Cr-40 at.% Al alloy. Philosophical Magazine Letters, 2000, 80, 703-710.	0.5	9
260	Experimental and theoretical study of the electroluminescence temperature dependence of iron disilicide light-emitting devices. Thin Solid Films, 2004, 461, 219-222.	0.8	9
261	Tuning the electrical performance of metal oxide thin-film transistors via dielectric interface trap passivation and graded channel modulation doping. Journal of Materials Chemistry C, 2017, 5, 1206-1215.	2.7	9
262	First-principles formulation of spinel-like structured Li _(4â^'3x) Y _x Cl ₄ as promising solid-state electrolytes to enable superb lithium ion conductivity and matching oxidation potentials to high-voltage cathodes. Journal of Materials Chemistry A, 2021, 9, 14969-14976.	5.2	9
263	Sponge tofu-like graphene-carbon hybrid supporting Pt–Co nanocrystals for efficient oxygen reduction reaction and Zn-Air battery. International Journal of Hydrogen Energy, 2021, 46, 15561-15571.	3.8	9
264	Influence of Halide Choice on Formation of Lowâ€Dimensional Perovskite Interlayer in Efficient Perovskite Solar Cells. Energy and Environmental Materials, 2022, 5, 670-682.	7.3	9
265	Characterization of GeSi/Si Heteroepitaxial Layered Structures by Convergent Beam Electron Diffraction. Japanese Journal of Applied Physics, 1993, 32, 404-407.	0.8	8
266	Ultra-thin twin plates and growth domains in the γ phase as a product of the B2 phase decomposition in Ti–40 at.% Al–10 at.% V. Philosophical Magazine A: Physics of Condensed Matter, Structure, Defects and Mechanical Properties, 1997, 75, 657-676.	0.7	8
267	omega phase formation in a physically vapour-deposited Fe-Al alloy. Philosophical Magazine Letters, 1997, 76, 207-216.	O.5	8
268	An ordered long-period superlattice structure of the B2 lattice. Applied Physics Letters, 1999, 74, 2643-2645.	1.5	8
269	Heaterâ€Free and Substrateâ€Independent Growth of Vertically Standing Graphene Using A Highâ€Flux Plasmaâ€Enhanced Chemical Vapor Deposition. Advanced Materials Interfaces, 2020, 7, 2000854.	1.9	8
270	Fine Structure of β-FeSi2 Formed out of α- FeSi2 Decomposition: Metastable Phase Transformations. Journal of Materials Science Letters, 1998, 17, 1243-1245.	0.5	7

#	Article	IF	CITATIONS
271	Influence of 2.8% zirconium addition on the microstructure of rapidly solidified Al-8Fe-4Ni alloy. Materials Science & Engineering A: Structural Materials: Properties, Microstructure and Processing, 1999, 267, 60-70.	2.6	7
272	Ion beam synthesis of gallium nitride. Nuclear Instruments & Methods in Physics Research B, 2001, 175-177, 678-682.	0.6	6
273	Dislocation-engineered silicon light-emitting diodes. , 2002, , .		6
274	A Potential Integrated Low Temperature Approach for Superconducting <tex>\$rm MgB_2\$</tex> Thin Film Growth and Electronics Device Fabrication by Ion Implantation. IEEE Transactions on Applied Superconductivity, 2005, 15, 3265-3268.	1.1	6
275	Numerical investigation of copper oxide-based heterojunction solar cells. Journal Physics D: Applied Physics, 2019, 52, 275105.	1.3	6
276	Planar Li growth on Li21Si5 modified Li metal for the stabilization of anode. Journal of Materials Science and Technology, 2021, 76, 156-165.	5.6	6
277	Effect of coating composition on the micro-galvanic dissolution behavior and antifouling performance of plasma-sprayed laminated-structured Cu Ti composite coating. Surface and Coatings Technology, 2021, 410, 126963.	2.2	6
278	Quasi-solid-state self-assembly of 1D-branched ZnSe/ZnS quantum rods into parallel monorail-like continuous films for solar devices. Nano Energy, 2021, 89, 106348.	8.2	6
279	Research on the Reversible and Irreversible Heat Generation of LiNi1â^'xâ^'yCoxMnyO2-Based Lithium-Ion Batteries. Fire Technology, 2023, 59, 1029-1049.	1.5	6
280	Enabling <scp>Highâ€Performance</scp> Sodium Battery Anodes by Complete Reduction of Graphene Oxide and Cooperative In‧itu Crystallization of Ultrafine <scp>SnO₂</scp> Nanocrystals. Energy and Environmental Materials, 2023, 6, .	7.3	6
281	On the crystallographic characteristics of ion-beam-synthesized Ru2Si3 precipitates. Applied Physics Letters, 2000, 76, 2529-2531.	1.5	5
282	Origin of Ferromagnetism in Co-Ion-Implanted Anatase TiO2Thin Films. Japanese Journal of Applied Physics, 2007, 46, 5767-5770.	0.8	5
283	Annealing and deposition temperature dependence of the bandgap of amorphous FeSi2fabricated by co-sputter deposition. Semiconductor Science and Technology, 2008, 23, 035007.	1.0	5
284	V and Ga Co-doping effect on optical absorption properties of TiO ₂ thin films. Journal of Physics: Conference Series, 2009, 152, 012073.	0.3	5
285	Enhanced Photoelectrochemical Performances in Flexible Mesoscopic Solar Cells: An Effective Lightâ€Scattering Material. ChemPhotoChem, 2018, 2, 986-993.	1.5	5
286	Large Scale Synthesis of Nanopyramidal-Like VO2 Films by an Oxygen-Assisted Etching Growth Method with Significantly Enhanced Field Emission Properties. Nanomaterials, 2019, 9, 549.	1.9	5
287	Hybrid Multipixel Array X-Ray Detectors for Real-Time Direct Detection of Hard X-Rays. IEEE Transactions on Nuclear Science, 2020, 67, 2238-2245.	1.2	5
288	Tailoring the Micro-galvanic Dissolution Behavior and Antifouling Performance Through Laminated-Structured Cu-X Composite Coating. Journal of Thermal Spray Technology, 2021, 30, 1566-1581.	1.6	5

#	Article	IF	CITATIONS
289	High Mobility and Photoâ€Bias Stable Metal Oxide Thinâ€Film Transistors Engineered by Gradient Doping. Advanced Electronic Materials, 2022, 8, .	2.6	5
290	Entropy Change Characteristics for Sodium Ion Half/Full Cells Based on Na ₃ V ₂ (PO ₄) ₃ and Hard Carbon Materials. Journal of the Electrochemical Society, 2022, 169, 050503.	1.3	5
291	Heat Generation and Temperature Rise Characteristics of Single Overcharged Lithium-Ion Batteries. Journal of the Electrochemical Society, 2022, 169, 060502.	1.3	5
292	The lamellar γ + β structure in Al-30T1-20V alloy. Scripta Metallurgica Et Materialia, 1995, 33, 13-17.	1.0	4
293	Properties of \hat{I}^2 -FeSi2 grown by combined ion irradiation and annealing of Fe/Si bilayers. Nuclear Instruments & Methods in Physics Research B, 2001, 175-177, 309-313.	0.6	4
294	The properties of β-FeSi2 fabricated by ion beam assisted deposition as a function of annealing conditions for use in solar cell applications. Nuclear Instruments & Methods in Physics Research B, 2002, 188, 179-182.	0.6	4
295	TEM observation of β-FeSi2(110),(101)/Si(111) layers grown by reactive deposition epitaxy in the presence of an Sb flux. Journal of Crystal Growth, 2002, 237-239, 249-253.	0.7	4
296	The roles of thermodynamics and transformation kinetics on phase selection in the non-equilibrium processing of materials. Materials Science & Engineering A: Structural Materials: Properties, Microstructure and Processing, 2004, 375-377, 556-560.	2.6	4
297	Dislocation engineering for Si-based light emitting diodes. Materials Science and Engineering B: Solid-State Materials for Advanced Technology, 2005, 124-125, 86-92.	1.7	4
298	Dislocation engineered silicon light emitting devices. Thin Solid Films, 2007, 515, 8113-8117.	0.8	4
299	Formation of dislocation loops in silicon by ion irradiation for silicon light emitting diodes. Nuclear Instruments & Methods in Physics Research B, 2008, 266, 2470-2474.	0.6	4
300	Melting of metallic and intermetallic solids: An energetic view from DFT calculated potential wells. Computational Materials Science, 2008, 43, 1141-1146.	1.4	4
301	Crystallographic characteristics and fine structures of semiconducting transition metal silicides. Thin Solid Films, 2011, 519, 8446-8450.	0.8	4
302	Rapid densification of SiC ceramic rollers by microwave sintering. Advances in Applied Ceramics, 2015, 114, 28-32.	0.6	4
303	A Novel Strategy for the Synthesis of CeO2/CeF3 Composite Powders with Improved Suspension Stability and Chemical Mechanical Polishing (CMP) Performance. Arabian Journal for Science and Engineering, 2015, 40, 2897-2901.	1.1	4
304	Graded Channel Junctionless InGaZnO Thin-Film Transistors with Both High Transporting Properties and Good Bias Stress Stability. ACS Applied Materials & Interfaces, 2020, 12, 43950-43957.	4.0	4
305	Dislocation-Based Silicon Light Emitting Devices. , 2003, , 11-20.		4
306	Energy level matching between transparent conducting electrodes and the electronic transport layer to enhance performance of all-inorganic CsPbBr3 solar cells. Vacuum, 2022, 200, 111028.	1.6	4

#	Article	IF	CITATIONS
307	The Nature of Active Sites for Plasmonâ€Mediated Photothermal Catalysis and Heatâ€Coupled Photocatalysis in Dry Reforming of Methane. Energy and Environmental Materials, 2023, 6, .	7.3	4
308	Coarsening and properties of extruded Al-8Fe-4Ni-1Mo alloys. Journal of Materials Science, 1994, 29, 1686-1691.	1.7	3
309	Diffraction from long-period out-of-phase superstructures. Intermetallics, 2002, 10, 493-496.	1.8	3
310	Phase selection in non-equilibrium processed TM–Al intermetallic alloys. Materials Science & Engineering A: Structural Materials: Properties, Microstructure and Processing, 2004, 375-377, 201-206.	2.6	3
311	Structural, electronic, and optical properties of Mn 4 Si 7. , 2008, , .		3
312	Role of nucleation in phase competition in binary Ti-Al alloys. Materials Science and Technology, 1997, 13, 797-805.	0.8	3
313	A transmission electron microscopy investigation of a metastable phase formed in rapidly solidified Al-Fe-Ti alloy. Journal of Materials Science Letters, 1993, 12, 1441-1443.	0.5	2
314	Reactive close field unbalance magnetron sputter deposition of titanium dioxides for potential photovoltaic applications. Surface Engineering, 2017, 33, 642-647.	1.1	2
315	One-dimensional Z-scheme TiO _{2/WO_{3 composite nanofibres for enhanced photocatalytic activity of hydrogen production. International Journal of Nanomanufacturing, 2019, 15, 227.}}	0.3	2
316	Dualâ€Modified Hollow Spherical Shell MoS 2 @TiO 2 /TiN Composites for Photocatalytic Hydrogen Production. Energy Technology, 0, , 2100265.	1.8	2
317	Self-aligned stitching growth of centimeter-scale quasi-single-crystalline hexagonal boron nitride monolayers on liquid copper. Nanoscale, 2022, , .	2.8	2
318	The electronic stability of tin-halide perovskite charged regions. Materials Advances, 2022, 3, 2524-2532.	2.6	2
319	Microstructural and mechanical evolution of amorphous Zr-Si with irradiation induced atomic reconfiguration and free volume variation. Surfaces and Interfaces, 2022, 30, 101890.	1.5	2
320	Metastable Phase Transformations in Ti-40Al-10V Alloy. Materials Research Society Symposia Proceedings, 1994, 364, 187.	0.1	1
321	Calculation of Phase Competition and Selection in Solidification Using a Combined Nucleation and Calphad Approach. Materials Research Society Symposia Proceedings, 1995, 398, 45.	0.1	1
322	Transient Nucleation Effects on Extension of Solid Solubility in Al-Ti and Al-Zr Alloys. Materials Science Forum, 1996, 217-222, 229-234.	0.3	1
323	Structural characterisation of ion beam synthesised Ru2Si3. Nuclear Instruments & Methods in Physics Research B, 2000, 161-163, 937-940.	0.6	1
324	Microstructure of (100) silicon wafer implanted by 1 MeV Ru+ ions. Journal of Materials Science, 2001, 36, 321-327.	1.7	1

#	Article	IF	CITATIONS
325	Zifâ€Derived Electrocatalysis: Dual Evolution in Defect and Morphology of Singleâ€Atom Dispersed Carbon Based Oxygen Electrocatalyst (Adv. Funct. Mater. 19/2021). Advanced Functional Materials, 2021, 31, 2170132.	7.8	1
326	X-ray photoelectron spectroscopy studies of Ti–Al and Ti–Al–V alloys using Cr Kβ radiation. , 2001, 31, 734.		1
327	TEM investigation of rapidly quenched metastable Î ³ TiAl phases. European Physical Journal Special Topics, 1993, 03, C7-465-C7-468.	0.2	1
328	One-dimensional Z-scheme TiO _{2/WO_{3 composite nanofibres for enhanced photocatalytic activity of hydrogen production. International Journal of Nanomanufacturing, 2019, 15, 227.}}	0.3	1
329	On the thermal stability and oxidation resistance of Zr/X(Cr, Ni, Si) multilayer structure. Surface and Coatings Technology, 2022, 440, 128500.	2.2	1
330	The Effects of Composition on the Spectral Loss Characteristics of SiGe Planar Waveguide Structures. Materials Research Society Symposia Proceedings, 1992, 281, 461.	0.1	0
331	Solidification of Al-7Si-2Ti-2Ce Alloy Ribbons. Materials Science Forum, 1996, 217-222, 213-218.	0.3	0
332	Efficient optical sources in silicon using dislocation engineering. , 2002, , .		0
333	TEM and PL Study of FeSi2 Precipitates Formed in Si by Iron Implantation Using a Metal Vapor Vacuum Arc Ion Source. Materials Research Society Symposia Proceedings, 2002, 737, 683.	0.1	0
334	Effect of implant conditions on the optical and structural properties of &beta;-FeSi ₂ . , 2002, , .		0
335	Efficient silicon light emitting diodes made by dislocation engineering. Materials Research Society Symposia Proceedings, 2002, 719, 511.	0.1	0
336	Ferromagnetism in transition metal-implanted titanium dioxide films. , 2004, , .		0
337	Photoluminescence and electroluminescence properties of FeSi2-Si structures formed by MEVVA implantation. Materials Research Society Symposia Proceedings, 2005, 862, 971.	0.1	0
338	Dislocation engineered silicon for light emission. , 2005, , .		0
339	Structures and light emission properties of ion beam synthesized FeSi 2 in silicon. , 2005, , .		0
340	Microstructure and Mechanical Properties of Fe-Containing Al-Alloys Processed by a Rheo-Diecasting Process. Materials Science Forum, 2006, 519-521, 1251-1256.	0.3	0
341	Microstructual and optical properties of novel Fe _{1-x} Os _x Si ₂ semiconducting alloys. Journal of Physics: Conference Series, 2009, 152, 012011.	0.3	0
342	Thermal and structural study of nanocrystalline Fe(Co)NiZrB alloys prepared by mechanical alloying. Journal of Materials Science, 2010, 45, 557-561.	1.7	0

#	Article	IF	CITATIONS
343	Fabrication and characterization of novel Fe(Os)Si2 semiconductor. Physics Procedia, 2011, 11, 75-78.	1.2	0
344	Hierarchical Porous Materials: Multidimensionâ€Controllable Synthesis of Ant Nestâ€6tructural Electrode Materials with Unique 3D Hierarchical Porous Features toward Electrochemical Applications (Adv. Funct. Mater. 29/2019). Advanced Functional Materials, 2019, 29, 1970196.	7.8	0
345	THE POTENTIAL OF \hat{l}^2 -		0
346	TEM studies of dislocation-based silicon light emitting devices. , 2004, , 113-116.		0
347	Interpretation of diffraction patterns from long-period out-of-phase superlattice structures. , 2004, , 209-212.		0
348	Characterization of GeSi/Si Layer Structure by CBED. , 1992, , .		0
349	Solidification and metastable phase formation in conventional and planar flow cast Ti-48.8at%Al-2.2at%V. European Physical Journal Special Topics, 1993, 03, C7-377-C7-382.	0.2	0
350	Lead-Free Perovskite Solar Cells with Efficiencies Reaching 8.29% Based on Single-Crystalline Precursor Solutions. SSRN Electronic Journal, 0, , .	0.4	0
351	Introduction of Frontier Outlook. Energy and Environmental Materials, 2022, 5, 5-5.	7.3	0
352	Editor's Note on "Frontier Outlook―Column. Energy and Environmental Materials, 2022, 5, 365-365.	7.3	0